DALHOUSIE UNIVERSITY

Investigation of the Stress-Strain Constitutive Behavior of ±55° Filament Wound GFRP Pipes in Compression and Tension

Dillon Betts[1], Pedram Sadeghian[1*], and Amir Fam[2]

[1] Department of Civil and Resource Engineering, Dalhousie University, 1360 Barrington St., Halifax, NS, B3H 4R2, Canada

[2] Department of Civil Engineering, Queen's University, 58 University Ave., Kingston, ON, K7L 3N6, Canada

[*] Corresponding Author: Pedram.Sadeghian@dal.ca

ABSTRACT: The behavior of hollow ±55º filament wound glass fiber-reinforced polymer (GFRP) pipes under longitudinal compressive and tensile loading is studied experimentally using 31 pipe specimens. The main parameters were the nominal pipe pressure rating, namely 350 kPa, 700 kPa and 1050 kPa, and the inner diameter, namely 76 mm and 203 mm. For the compression tests, each specimen was cut to a length of twice the outer diameter and the ends were protected from premature failure using a basalt fiber-reinforced polymer (FRP) wrap. A spherical platen was used to ensure concentric loading. For the tensile tests, a novel test set-up with a specialized gripping mechanism was used to test the full pipe in lieu of the standard coupons extracted from the pipe which suffer from fiber discontinuity, thereby underestimating the strength. The pipes exhibited a nonlinear stress-strain response under both tension and compression loads and exhibited a higher strength in compression than in tension. Additionally, the pipes showed a significant post-peak behavior when loaded in tension. An analytical model capable of representing the behavior of FRPs under axial tension and compression using simplified constitutive relations was adopted and applied. The proposed model captures the nonlinear stress-strain behavior of the hollow pipes in tension and compression as well as the post-peak behavior of the pipes in tension. The effects of fiber angle error are also explored.

Understanding the material behavior is important when analyzing these pipes under flexural or axial loading or when analyzing structures using these pipes, such as concrete-filled FRP tubes (CFFTs).

https://doi.org/10.1016/j.compositesb.2019.05.077

KEYWORDS: GFRP Pipes, Angle-ply, Tension, Compression, Experimental, Analysis.

1. INTRODUCTION

The use of fiber-reinforced polymers (FRPs), such as glass FRPs (GFRPs), has become popular in sustainable infrastructure applications. They can take a variety of forms, including pipes which can be filled with concrete and used as structural members subjected to flexure and axial loading, where the GFRP pipe provides significant confinement for concrete column applications. These structural systems are typically referred to as "concrete-filled FRP tubes", or CFFTs. For these structural systems, it is important to understand the macroscopic behavior of hollow GFRP pipes under structural loading, such as axial compression and tension.

Filament wound GFRP pipes are often used in the piping industry for oil and gas or municipal applications and there are numerous studies on their resistance to internal pressure [1–3]. There have also been studies on similar pipes under pure axial tensile loading [2,4] and on the combined biaxial loading [5–8], one of which presented the pure axial compression behavior [8]. However, studies on the axial behavior of these pipes are quite scarce, especially under axial compression. Their structural properties are still not fully identified or understood, especially the nonlinear behavior arising from the angle-ply structure.

It is also important to be able to predict the behavior of these pipes under structural loading. Therefore, an analytical technique based on the procedure proposed by Petit and Waddoups [9] was developed for the GFRP pipes. Mallick [10] stated that the stress-strain softening of ±θ° (angle-ply) FRP pipes is attributed to the nonlinear behavior of the laminae under shear loading. Therefore, the model considers the nonlinear shear behavior of the laminae to accurately predict the stress-strain behavior of the GFRP filament wound pipes under pure tensile and compressive loading. Lin and Hu [11] developed a model that included a shear parameter to incorporate the shear stress-strain nonlinearity into the model. This analysis was based on the procedures proposed by Hahn and Tsai [12] and Hahn [13]. To use the model by Lin and Hu [11], the shear parameter must be determined by fitting a curve to shear stress-strain test data. In the current study, the model by Petit and Waddoups [9] was chosen due to the accuracy resulting from the use of the actual material behavior at each model increment. The model incorporates the nonlinear material behavior in each direction by using tangent moduli at each model increment determined from each respective stress-strain relationship.

In the current study, the behavior of ±55° filament wound GFRP pipes under pure axial compression and pure axial tension will be examined. The fiber architecture of ±55° was chosen due to the commercial availability of such GFRP pipes due to their use in the pipeline industry. Therefore, because ±55° pipes are readily available in the market, they could provide an economic benefit if used in structural applications. It is understood that for structural applications, other fiber architectures would be more suitable; however, the intent of this study was to characterize commercially available pipes. Pipes with different nominal pressure ratings and pipe diameters were tested. The effect of these parameters on pipe stiffness and strength is discussed.

The results of the current study showed that ±55° GFRP pipes exhibited a nonlinear stress-strain response and that when loaded in tension there is a significant post-peak behavior. This post-peak

behavior was also observed in previous studies [2,4]. The model proposed in the current study captures the nonlinear behavior and the post-peak behavior of the GFRP pipes. Understanding this material level behavior of these pipes is important for analyzing similar pipes under pure flexural or combined axial and flexural loads and for analyzing structural systems which use these pipes, such as CFFTs.

2. RESEARCH SIGNIFICANCE

The goal of the current paper is to provide a better understanding of $\pm\theta°$ filament wound GFRP pipes, specifically ±55° GFRP pipes which are widely used and commercially available in the pipeline industry. The ±55° pipes are used in this industry because of their resistance to internal pressure forces. In the current study they are being examined for use in structural applications involving concrete filling. Though ±55° FRP structures are not typically suitable for applications tension or compression, when used for concrete-filled structures, their fiber architecture is beneficial for providing some concrete confinement while also providing axial and flexural resistance [14,15]. The macroscopic structural properties of these pipes are not well known. This is due to the fact that these pipes are predominately loaded circumferentially under internal fluid pressure and due to the difficulty in testing these pipes under longitudinal tension. The purpose of the current study is to characterize the mechanical behavior of these pipes for construction applications and, specifically, to capture the nonlinear behavior.

A novel test method involving a specialized gripping mechanism is developed and used to test the full pipe in tension, rather than the standard tension coupons extracted from the pipes. These coupons suffer from fiber discontinuity along the edges, leading to premature failure and underestimation of the pipe's mechanical properties. This occurs due to the v-notch failure mechanism that occurs

parallel to the fiber direction. The full pipe test method in the current study captures the actual tensile behavior of these pipes, including the ultimate tensile strength and post-peak behavior, which cannot be obtained from standard coupon tests.

3. EXPERIMENTAL PROGRAM

A total of 31 specimens were tested as part of this study: 25 compression specimens and six tension specimens. All pipes were supplied by the manufacturer (RPS Composites, Mahone Bay, NS, Canada). The pipes were manufactured using continuous roving ECR glass fibers and a BIS-A vinylester resin (Ashland Derakane 411). The fiber volume fraction of the pipes was 50.2% and they were manufactured with a fiber angle of ±55° with an error of ±2°. The compression specimen geometries and the tension specimen shapes were chosen to allow for uniform stress distribution at mid-height. Therefore, the average cross-sectional stress is representative of the actual stress experienced by the test specimens. This can be verified by finite element modelling in future studies.

3.1. Test Matrix

The test matrix is shown in Table 1. The specimen dimensions as well as the nominal pressure ratings were provided by the manufacturer. The filament stacking sequence and laminate structure were determined by a burn-off test, where a small section of each specimen type was heated with a torch until the resin was completely removed. The burn-off tests were performed to determine the number of layers of glass fibers in each specimen as reported in Table 1. This information was required to accurately model the behavior of the pipes. The main test parameter was the nominal pipe pressure rating (350 kPa, 700 kPa and 1050 kPa) which is a reflection of the different wall thicknesses and inner diameters (76.2 mm and 203.2 mm). Specimens were named according to the following convention: PX-DY-C/T-Z, where X is the pipe pressure rating in kPa (350, 700 or 1050), Y is the

nominal pipe diameter in mm (76 or 203), C/T is for compression/tension and Z is a sequential number to distinguish identical specimens.

3.2.Test Setup and Instrumentation

To determine both the tensile and compressive behavior of the pipes, two test methods were used: a compression test and a novel tension test. The tests were carried out using a 2MN Instron 5590-HVL Static Hydraulic Universal Testing System.

3.2.1. Compression Tests

A total of 25 compression tests were completed. The compression tests were based on the procedures in ASTM D5449 [16]. This standard was written for the testing of hoop wound cylinders but was adopted for the tests in this study. The aspect ratio was adjusted to 2:1 such that the ends did not affect the failure in the gauge length. For each pipe type, five specimens were cut from a 7620 mm long pipe supplied by the manufacturer using a band saw. The length of each specimen was twice its outer diameter. To avoid local crushing failure at the pipe ends, each end was reinforced using a basalt FRP (BFRP) wrap. Each basalt wrap was two plies thick, with an overlap length of one third the specimen circumference. The basalt wraps were 20 mm and 50 mm wide for the D76 type and D203 type specimens, respectively. The boundary conditions are extremely important when testing the compression behavior. This was accounted for both by grinding the ends of the specimens flat and the use of a spherical platen during testing.

The compression test set-up is shown in Figure 1. Each specimen was instrumented using four strain gauges applied to the outer surface of the pipe: two oriented parallel to the direction of loading (axial) and two oriented perpendicular to the direction of loading (hoop). A spherical platen was used at the bottom surface to account for any unevenness of the specimen ends. Each test was performed at a displacement rate of 0.6 mm/min. This displacement rate was used as it provided an adequate test

time for collecting data which is specified to be within one to ten minutes in ASTM D5449 [16]. The load, stroke and strain data were sampled at a rate of 10 Hz. A photo of all compression test specimens is presented in Figure 2.

3.2.2. Tension Tests

A total of six tension specimens were tested. The tensile specimens were made specifically for testing by the manufacturer and, for this reason, only a limited amount were available. To ensure failure occurred within the gauge length of the tensile pipes, the specimens were made into a "dumbbell" (or "dog bone") shape as shown in Figure 3. Each end was fitted with a 75.6 mm diameter, 126.5 mm long steel core using four 12.7 mm diameter cap screws, tightened by hand. Additionally, five stainless steel pipe straps (12.7 mm wide and 0.7 mm thick) were used to increase the friction between the steel core and the inside of the pipe. A 25.4 mm diameter steel rod extended 320 mm longitudinally from the steel core which was gripped by the test machine. The steel rod was free to rotate about the loading axis, such that there was no transfer of bending into the specimen.

The tension test set-up is shown in Figure 3. The novel test set-up was used in place of the standard ASTM D2105 [17], because the standard test fixture was prone to slipping before specimen failure. Each specimen had a gauge length of 400 mm and was instrumented with a total of six strain gauges: four applied in the axial direction and two in the hoop direction. The tests were performed at a rate of 2 mm/min, such that the test reached a peak load with a time limit of one to ten minutes. The load, stroke and strain data were sampled at a rate of 10 Hz. The tension tests were stopped when the load decreased to 80% of the observed peak load. A photo of all tension specimens is shown in Figure 4.

4. EXPERIMENTAL RESULTS AND DISCUSSIONS

Based on the recorded load and strain data, the engineering stress-strain behavior of each pipe specimen was determined, and the strength and pipe modulus were calculated. The data processing was performed by a Python program written using the scientific programming package, Anaconda. Python was used because it is more repeatable and can process larger data sets better than traditional spreadsheets, permitting faster data processing. The data was recording using a data acquisition unit and stored in tab delimited ASCII text files, which can then be read and plotted using the python code. The engineering stress was calculated based on the load data and the original cross-sectional areas provided by the pipe manufacturer shown in Table 1.

For all pipes (both tension and compression specimens), the pipe moduli were found by determining the slope of a linear fit to the axial stress-strain data between strain values of 0.0004 mm/mm and 0.0013 mm/mm, unless another portion better represented the first linear portion as per ASME RTP-1 [18]. The Poisson's Ratios were found by finding the slope of the hoop stress-strain data in the same period and dividing the pipe moduli by this slope. They are presented in Table 2 and ranged from 0.41 (P1050-D76-T) to 0.61 (P700-D76-C). Based on the results, it seems that neither nominal pressure rating nor pipe diameter had a significant effect on the Poisson's Ratio and the average Poisson's Ratio of all specimen types was 0.48 ± 0.07.

4.1. Compression Behavior

Five identical specimens of each pipe type were tested under uniaxial compression. The stress-strain behavior of all compression tests is presented in Figure 5. The test results are presented in Table 2. Note that the exact ultimate strain of the specimens cannot be presented as strain gauge failure occurred prior to ultimate failure; however, the specimens failed shortly after the strain gauges and therefore the plots show the test data until strain gauge failure only.

Generally, all pipes failed in a similar manner. Failure started with matrix cracking parallel to the fiber direction and continued until ultimate failure by crushing. The only specimen group that did not follow this trend was P350-D203. These specimens failed prematurely due to localized buckling of the pipe wall, as will be discussed in the proceeding sections.

4.1.1. Effect of Diameter – Wall Thickness Ratio

As presented in Table 1, the Diameter-Thickness Ratios (DTR) varied from 20.1 (P1050-D76) to 75.3 (P350-D203). Specimens with a DTR of 75.3 showed a significant reduction in strength when compared to specimens with lower DTR values (20.1 – 44.8). This strength reduction was caused by premature local buckling which was observed during testing. For the 203.2 mm diameter pipes, a single factor analysis of variation (ANOVA) to compare specimen strengths showed with 95% confidence that decreasing the DTR from 43.2 to 30.3 had no significant effect on the pipe strength. On average the P350-D203 failed at a compressive stress of 73.3 MPa, whereas the P700-D203 pipes failed at an average stress of 114.7 MPa, which is an increase of 56%. Similarly, the P1050-D203 pipes exhibited an increase in strength of 60% when compared with the P350-D203 pipes. Pipes with the lowest DTR of 20.1 (P1050-D76) showed an increase in strength when compared to pipes with the next-lowest DTR of 30.3 (P1050-D203). The ultimate capacity increased from 117.2 MPa to 128.9 MPa, an increase of 10%. Generally, strength decreased as DTR increased, however no significant effect was observed when the DTR was between 30.3 and 44.8.

Based on single factor ANOVA analyzes with a confidence of 95%, the only significant difference between moduli of the D203 pipes was between that of specimen types P350-D203 (DTR of 75.3) and P1050-D203 (DTR of 30.3). The pipe modulus decreased by 28% as pipe pressure rating increased, decreasing from 11.50 GPa (P350-D203) to 8.32 GPa (P1050-D203). Though not

statistically significant due to the high variability of the data, P700-D203 fit the decreasing trend with an average pipe modulus of 10.03 GPa.

4.2. Tension Behavior

A total of six 76.2 mm diameter pipe specimens were tested in uniaxial tension as a part of this study: three P350 pipes (DTR of 44.8) and three P1050 pipes (DTR of 20.1). The stress-strain plots of all tests are shown in Figure 6. The pipes with a lower DTR (i.e. P1050 pipes) exhibited higher strength and stiffness than the pipes with a higher DTR (i.e. P350). The average tensile strength increased from 47.5 MPa to 70.8 MPa (an increase of 49%) and the average pipe modulus increased from 8.68 GPa to 10.68 GPa (an increase of 23%). One hypothesis for this behavior is that during tensile loading the diameter at mid-height is reduced which induces longitudinal bending of the wall. This phenomenon would likely have less of an effect on the pipes with thicker walls than the pipes with thinner walls. Another hypothesis for this behavior is that the thinner P350 pipes did not have enough fibers. This could have caused a premature softening of the pipes due to matrix cracking in the resin rich areas. Due to the difference in properties of the composites and resins in tension and compression, this behavior would not necessarily have been observed in compression. Both hypotheses require further research to determine the actual cause of the reduction in strength in pipes with thinner walls. The first hypothesis can be tested through a detailed finite element model considering geometric nonlinearities to obtain the effect of secondary moments. This finite element model could then be further verified using additional tests measuring the change in diameter using digital image correlation. The second hypothesis could be investigated through further testing of pipes with a nominal pressure rating of 700 kPa.

The pipes did not experience an ultimate failure during the tension tests. The tests were stopped minimum reduction in load of 20% of the peak load. During the tests, the strain gauges failed shortly

after the peak load was reached, however the pipes continued to elongate. To further understand the post-peak behavior of the pipes, the stroke data was calibrated based on the available strain data and plotted with the stress-strain data, as presented in Figure 6. Understanding this post-peak behavior is important when analyzing these pipes in other applications, such as bending.

4.3. Comparison of Compressive and Tensile Behavior

Figure 7 shows a comparison of the axial stress-strain behavior of the tension and compression tests. All compression tests exhibited a higher level of strain before ultimate failure than their tensile counterparts. The pipes were also shown to be stronger in compression than in tension. Pipes with a nominal pressure rating of 350 kPa were 167% stronger in compression than in tension on average. The 1050 kPa pipes also exhibited higher strength in compression, an 83% increase in strength compared to the tensile specimens.

5. ANALYTICAL STUDY

This section presents the results of a model used to predict the behavior of ±θ° FRP pipes under both axial compression and tension. Petit and Waddoups [9] used the stress-strain results of FRPs tested in different configurations (ie. axial, transverse, shear) to determine a tangent modulus in each direction. These moduli were used at each model increment to determine the behavior of flat laminates using an incremental Classical Lamination Theory (CLT) analysis. For the current study, the model by Petit and Waddoups [9] was adopted and used to predict the behavior tubular FRP structures.

In this study, only the transverse and shear behavior of the lamina were considered to be nonlinear and were modelled as parabolic and cubic relationships, respectively. Based on the models of the material in the transverse and shear directions, tangent moduli are used to perform an incremental

CLT analysis. Additionally, based on the test data, a linear stress-strain relationship is proposed for the post-peak behavior of ±55° GFRP pipes under pure tensile load.

5.1. Nonlinear Mechanical Behavior

All pipes tested exhibited nonlinear mechanical behavior. Mallick [10] stated that the nonlinearity of ±θ° laminates is typically a stress-strain softening due to the shear stresses in the laminate. As expected, the test data of the filament wound pipes exhibits this behavior. Therefore, to accurately predict the stress-strain behavior of these pipes, it is important to include the nonlinearity of the shear stress-strain behavior of the laminate. To predict the nonlinear behavior of GFRP filament wound pipes under axial loading a nonlinear model for flat plates proposed by Petit and Waddoups [9] was adopted.

5.2. Analysis Description

To predict the behavior of ±θ° filament wound pipes, a computer program was written in the scientific Python package, Anaconda, to perform the nonlinear analysis. The program takes into account the unidirectional properties of the laminae, the loading type (i.e. tension or compression), the number of laminae and the geometric properties of the pipe as inputs. The program applies an initial load of 1000 N/mm and performs a CLT analysis to determine the stresses and strains developed in the laminate and checks the stresses against the maximum stress criteria. The program runs in a loop, increasing the applied load in increments of 1000 N/mm until laminate failure. The output of the program is a stress-strain plot and a maximum axial strength of the pipe in either tension or compression.

For the analysis of compression tests, the program also calculates the start of a potential buckling zone based on Eq. 1 presented by Timoshenko and Gere [19] for the calculation of critical buckling stress in thin shells.

$$\sigma_{cr} = \frac{E_t t}{r\sqrt{3(1-\nu^2)}} \quad (1)$$

where σ_{cr} is the critical stress to cause buckling, E_t is the tangent axial pipe modulus, determined by finding the slope between the stress-strain point calculated during each model increment (*i*) and the previous model increment (*i-1*), *t* is the pipe wall thickness (including liner and resin coat), *r* is the radius to the mid-plane of the pipe wall, and *v* is the Poisson's ratio of the pipe. This critical buckling stress equation was developed for isotropic materials [19], and therefore, as only the axial modulus of elasticity is used, it provides only an estimation of when buckling could occur, for discussion. The critical buckling stress was calculated at each model increment and compared to the axial stress in the pipe at that increment. The start of the potential buckling zone was then determined when the critical buckling stress was less than or equal to the axial stress in the pipe.

The assumed cross-section of the pipe wall used for modelling is shown in Figure 8. The filament wound laminae thicknesses were assumed to be the overall section thickness less the resin coat and the liner. The thickness of each lamina was considered to be the thickness of the filament wound core divided by the number of laminae.

5.3. Lamina Properties

The unidirectional properties of the GFRP laminae were assumed based on the properties provided by Daniel and Ishai [20] for an E-glass and epoxy resin lamina with a fiber volume fraction of 55%, as there were no strength properties available from the current pipe manufacturer. To more closely match the pipes in this study, the values from Daniel and Ishai [20] were adjusted to represent a composite with a volume fraction of 50% using Rule of Mixtures. The input data used in the model is compared with the available data from the manufacturer in Table 3. The values of longitudinal modulus, transverse modulus and shear modulus were within -9.3%, 5.6% and 21.3% of the

manufacturer's pipe data, respectively. Both the resin coating and the liner were considered as layers of pure epoxy resin, for simplicity.

As mentioned previously, the properties of ±55° laminates are heavily dependent on the shear stress-strain relationship. Therefore, to accurately predict the stress-strain behavior of the laminate, it is important to consider this relationship when performing the CLT analysis. Therefore, a cubic model was developed to determine the slope of the shear stress-strain (G_{12}) plot at any level of shear strain. The cubic model was developed based on Eq. 2.

$$\tau = A_1\gamma^3 + B_1\gamma^2 + C_1\gamma + D_1 \quad (2)$$

Parameters A_1, B_1, C_1, and D_1 were constants solved using the following boundary conditions: $\{\gamma = \gamma_u; \tau = \tau_u\}$; $\{\gamma = 0; \tau = 0\}$; $\{\gamma = \gamma_u; d\tau/d\gamma = G_{12o}/10\}$; and $\{\gamma = 0; d\tau/d\gamma = G_{12o}\}$, where γ_u is the ultimate shear strain of the lamina, τ_u is the ultimate shear strength of the lamina, and G_{12o} is the initial shear modulus of the lamina presented in Table 3. The third boundary condition was chosen based on the shear stress-strain of the glass/epoxy FRP data in the study by Puck and Mannigel [21]. The data from their study showed that the final slope of the shear stress-strain plot was approximately 10% of the initial shear modulus G_{12o}. The proposed cubic model was fit to the data from Puck and Mannigel [21] and is presented in Figure 9a. The model used for this paper is shown in Figure 9b. The ultimate shear strain was not provided by Daniel and Ishai [20] and therefore the ultimate shear strain of 0.04 mm/mm was chosen based on the test data from Puck and Mannigel [21]. The equation for shear strength and modulus at any shear strain level are shown in Eq. 3 and Eq. 4, respectively.

$$\tau = \frac{2}{\gamma_u^3}[0.55G_{12o}\gamma_u - \tau_u]\gamma^3 + \frac{1}{\gamma_u^2}[3\tau_u - 2.1G_{12o}\gamma_u]\gamma^2 + G_{12o}\gamma \quad (3)$$

$$G_{12} = \frac{6}{\gamma_u^3}[0.55G_{12o}\gamma_u - \tau_u]\gamma^2 + \frac{2}{\gamma_u}[3\tau_u - 2.1G_{12o}\gamma_u]\gamma + G_{12o} \quad (4)$$

During each iteration of the program loop, the shear modulus, G_{12}, is calculated based on the shear strain from the previous loop. Similarly, the nonlinear tensile behavior of the composite in the transverse direction was considered. The compressive behavior of the composite in the transverse direction was considered to be linear-elastic until failure due to a lack of information concerning the stress-strain behavior. It was determined that the transverse tensile behavior could be modelled simply with a parabolic curve governed by Eq. 5.

$$\epsilon_2 = A_2{\sigma_2}^2 + B_2{\sigma_2}^2 + C_2 \quad (5)$$

Parameters A_2, B_2 and C_2 are constants determined using the following boundary conditions: $\{\epsilon_2 = \epsilon_{2u}; \sigma_2 = \sigma_{2u}\}$; $\{\epsilon_2 = 0; \sigma_2 = 0\}$; and $\{\epsilon_2 = 0; d\sigma_2/d\epsilon_2 = E_{2o}\}$, where ϵ_{2u} is the ultimate transverse tensile strain, σ_{2u} is the ultimate transverse tensile strength and E_{2o} is the initial transverse tensile modulus. The tangent transverse tensile modulus was determined at each loop iteration using Eq. 6 and the transverse stress (σ_2) calculated based on the previous loop iteration. The parabolic model was verified using transverse stress-strain data from a study by Benzarti et al. [22] which is presented in Figure 9c. The parabolic model used for this study is presented in Figure 9d.

$$E_2 = \frac{\sigma_{2u}}{2\sigma_2\left(\frac{\epsilon_{2u}}{\sigma_{2u}} - \frac{1}{E_{2o}}\right) + \frac{\sigma_{2u}}{E_{2o}}} \quad (6)$$

Based on the tangent shear modulus and the tangent transverse tensile modulus, the stiffness matrix, [Q], for each lamina is recalculated at each loop iteration and the stiffness of the entire laminate is reduced thereby providing the expected softening effect.

As discussed earlier, the pipe tension tests showed a significant post-peak behavior. From Figure 6, it can be seen that the post-peak behavior is approximately linear. Therefore, in order to capture

this behavior in the model, a linear descending branch was added to the tension model after ultimate stress. Based on the test data, the post-peak model was set to decrease from σ_u to 60% of σ_u at a slope $0.08(\sigma_u/\epsilon_u)$. This is further verified in the next section.

5.4. Verification

Figure 10 and Figures 11 and 12 show the verification of the model against the compression test data and the tension test data, respectively. Table 2 shows a comparison of the test and model results. Generally, the nonlinear behavior of the filament wound pipes can be predicted well using the nonlinear model.

Based on Figure 10 and Table 2, the compression model fits the data well. Note that model overpredicts the failure of the P350-D203 pipes. However, as this pipe experienced premature failure due to local buckling, this was expected. As the model assumes material failure, it does not capture stability failure mechanisms. However, the potential start of a buckling zone was calculated using Eq. 1 and is presented in Figure 10. Because this equation is based on the tangent modulus, all pipes are shown to have the start of potential buckling occur when the pipe modulus is significantly reduced. The prediction of the potential buckling is shown to match the failure location of the P305-D203 pipes well.

Figure 11 and Table 2 show that the moduli of the tension models match those of the tests well. Additionally, the strength of P1050-D76-T is close to that of the tests, the test/model ratio being 0.92. However, the strength of P350-D76-T was overpredicted. This was expected as the results of the tests were much lower than the P1050-D76-T specimens. One hypothesis for this discrepancy is that the pipes failed prematurely due to stability or a lack of uniform fibers distribution in each layer. Figure 12 shows that the assumed post-peak slope matches the data well. As this portion of the model is

based on the test data of the current study, it should be verified using more tests of pipes with different angle-ply structures.

The analytical model was further verified using data from the available literature. The compression tests of ±55° pipes by Kaddour et al [8] and the tension tests of ±55° pipes by Bai et al [2] were modelled and are presented with the original data in Figure 13. The glass/epoxy pipes tested by Kaddour et al [8] had an inner diameter of 100 mm and a wall thickness of 9.57 mm (DTR = 10.4). To model these pipes, the properties of the GFRPs presented in their study were used, however no information on the ultimate shear strain was available. Therefore, the ultimate shear strain was assumed to be 0.04 mm/mm based on the data from Puck and Mannigel [21] as in the current study. The compression model shown in Figure 13a captures the initial stiffness of the tests by Kaddour et al [8] well, however it underpredicts the ultimate strength. As the model is significantly affected by the shear behavior of the GFRPs, the assumption used for the ultimate shear strain could be the cause of this underprediction. A more accurate model could be developed knowing the actual properties of the GFRPs in shear.

The model of the tension tests of the glass/epoxy pipes by Bai et al [2] is presented in Figure 13b. The pipes tested in the study had an inner diameter of 60 mm and a wall thickness of 2.5 (DTR = 24). No GFRP properties were presented in the study, but the nominal fiber volume fraction was reported to be 56%. Therefore the GFRP properties presented by Daniel and Ishai [20] and given in Table 3 were used. The tension tests by Bai et al [2] also show a significant post-peak behavior and exhibited similar behavior to the pipes in the current study. The tension data model, including the post-peak portion, fits the data of both the tests in the current study and the tests by Bai et al [2] well.

5.5. Parametric Study

Using the analytical model verified in the preceding section the stress-strain plots of GFRP filament wound pipes with fiber angles of ±53°, ±55° and ±57° were generated and are presented in Figure 14. These angles were chosen as the manufacturer reported a potential error of ±2° when manufacturing the pipes. This analysis was completed assuming that there was both a liner and a resin coat of pure epoxy, for simplicity. The figure shows that the specimen strength is increased with a decrease in fiber angle.

The research presented in this study can be used in the analysis and modelling of filament wound GFRP pipes used in other applications, such as CFFTs. Additionally, understanding the compression and tension behavior of these pipes is important for analysis and modelling of pipes under different loading conditions, such as pure flexural or combined axial and flexural loads. Future research in this area should therefore include testing and modelling ±55° GFRP pipes in different applications, such as CFFTs under axial loads, flexural loads, and combined loads.

6. CONCLUSIONS

In this study, 31 filament-wound GFRP pipe specimens were tested under uniaxial compression and tension. The main parameters of the tests were nominal pipe pressure rating (350 kPa, 700 kPa and 1050 kPa) which reflects a variation in wall thickness, and inner pipe diameter (76.2 mm and 203.2 mm). Five identical pipe specimens of each type were tested in compression and three identical pipe specimens of each type were tested in tension. A model was developed based on an existing method for flat plates. The existing model was adopted and applied to the analysis of tubular structures with a variety of fiber architectures, specifically ±θ°. Additionally, a linear prediction of the post-peak behavior of ± 55° GFRP pipes was proposed based on the test data. The model was able to predict the stress-strain behavior of the pipes and could also predict the ultimate strength and the pipe modulus. Based on the results of the testing and modelling, the following conclusions were made:

- In compression, pipe strength increased with a decrease in the diameter-thickness ratio (DTR). The most prominent reduction in strength was when DTR changed from 44.8 to 75.3. The specimens with DTR of 75.3 failed prematurely due to localized buckling which was observed during testing.
- In tension, the strength and stiffness increased with DTR. The strength and stiffness of P1050 specimens were 49% and 23% higher than the P350 specimens, respectively. However, it was hypothesized that this difference is due to a premature failure of the P350 pipes.
- The pipes exhibited a significant post-peak behavior when loaded in tension. This behavior was included in the model as a linear decrease with a slope of $0.08(\sigma_u/\epsilon_u)$.
- A nonlinear CLT analysis was used to predict the behavior of ±θ° pipes until the peak load. The model was able to capture the nonlinear behavior of the pipes and the ultimate load. The model was verified using data from the current study as well as two independent studies.
- A parametric study of the model showed that the strength and stiffness of the pipes increased with a decrease in fiber angle.
- The model, including the post-peak behavior, can be used in future applications to predict the behavior of concrete-filled ±θ° FRP pipes or to predict the behavior of hollow GFRP pipes under different loading conditions.

7. ACKNOWLEDGEMENTS

The authors would like to thank Jesse Keane, Brian Kennedy, Jordan Maerz, Brandon Fillmore, and Rainer MacKay for their assistance in the lab. The authors would also like to acknowledge and thank NSERC, Queen's University, and Dalhousie University for financial support and RPS Composites (Mahone Bay, NS, Canada) for providing the pipe specimens and in-kind support.

8. DATA AVAILABILITY

The raw/processed data required to reproduce these findings cannot be shared at this time due to technical or time limitations.

9. REFERENCES

[1] Xing J, Geng P, Yang T. Stress and deformation of multiple winding angle hybrid filament-wound thick cylinder under axial loading and internal and external pressure. Compos Struct 2015;131:868–77. doi:10.1016/j.compstruct.2015.05.036.

[2] Bai J, Seeleuthner P, Bompard P. Mechanical behaviour of ±55° filament-wound glass-fibre/epoxy-resin tubes: I. Microstructural analyses, mechanical behaviour and damage mechanisms of composite tubes under pure tensile loading, pure internal pressure, and combined loading. Compos Sci Technol 1997;57:141–53. doi:10.1016/S0266-3538(96)00124-8.

[3] Xia M, Takayanagi H, Kemmochi K. Analysis of multi-layered filament-wound composite pipes under internal pressure. Compos Struct 2001;53:483–91. doi:10.1016/S0263-8223(01)00061-7.

[4] Khalifa A Ben, Zidi M, Abdelwahed L. Mechanical characterization of glass/vinylester ±55° filament wound pipes by acoustic emission under axial monotonic loading. Comptes Rendus - Mec 2012;340:453–60. doi:10.1016/j.crme.2012.02.006.

[5] Mertiny P, Ellyin F, Hothan A. Stacking sequence effect of multi-angle filament wound tubular composite structures. J Compos Mater 2004;38:1095–113. doi:10.1177/0021998304042077.

[6] Mertiny P, Ellyin F, Hothan A. An experimental investigation on the effect of multi-angle

filament winding on the strength of tubular composite structures. Compos Sci Technol 2004;64:1–9. doi:10.1016/S0266-3538(03)00198-2.

[7] Ellyin F, Carroll M, Kujawski D, Chiu AS. The behavior of multidirectional filament wound fibreglass/epoxy tubulars under biaxial loading. Compos Part A Appl Sci Manuf 1997;28:781–90. doi:10.1016/S1359-835X(97)00021-3.

[8] Kaddour AS, Soden PD, Hinton MJ. Failure of ±55 Degree Filament Wound Glass/Epoxy Composite Tubes under Biaxial Compression. J Compos Mater 1998;32:1618–45. doi:10.1177/016344300022005001.

[9] Petit PH, Waddoups ME. A Method of Predicting the Non Linear Behaviour of Laminated Composites. J Compos Mater 1969;3:2–19.

[10] Mallick PK. Fiber-Reinforced Composites: Materials, Manufacturing and Design. Third. NW: CRC Press; 2007.

[11] Lin WP, Hu H-T. Nonlinear Analysis of Fiber-Reinforced Composite Laminates Subjected to Uniaxial Tensile Load. Jounal Compos Mater 2002;36:1429–50. doi:10.1106/002199802021463.

[12] Hahn HT, Tsai SW. Nonlinear Elastc Behaviour of Unidirectional Composite Laminae. J Compos Mater 1973;7:102–18.

[13] Hahn HT. Nonlinear behavior of laminated composite plates. J Compos Mater 1973;7:257–71.

[14] Zhu Z, Ahmad I, Mirmiran A. Seismic Performance of Concrete-Filled FRP Tube Columns for Bridge Substructure. J Bridg Eng 2006;11:359–70. doi:10.1061/(asce)1084-0702(2006)11:3(359).

[15] Mirmiran A, Shahawy M. A new concrete-filled hollow FRP composite column

1996;27:263–8. doi:10.1073/pnas.0504628102.

[16] ASTM. ASTM D5449, Transverse Compressive Properties of Hoop Wound Polymer Matrix Composite Cylinders. Annu B ASTM Stand 2016:1–10. doi:10.1520/D5449.

[17] ASTM. ASTM D2105, Longitudinal Tensile Properties of "Fiberglass" (Glass-Fiber-Reinforced Thermosetting-Resin) Pipe and Tube 2014;01:1–6. doi:10.1520/D2105-01R14.2.

[18] American Society of Mechanical Engineers. RTP-1 - 2011 - Reinforced Thermoset Plastic Equipment 2011.

[19] Timoshenko S, Gere J. Theory of Elastic Stability. Second Ed. McGraw-Hill; 1963.

[20] Daniel IM, Ishai O. Engineering mechanics of composite materials. Mech Compos Mater 1994. doi:10.1016/B978-0-08-006421-5.50049-6.

[21] Puck A, Mannigel M. Physically based non-linear stress-strain relations for the inter-fibre fracture analysis of FRP laminates. Compos Sci Technol 2007;67:1955–64. doi:10.1016/j.compscitech.2006.10.008.

[22] Benzarti K, Cangemi L, Dal Maso FD. Transverse properties of unidirectional glass/epoxy composites: Influence of fibre surface treatments. Compos Part A Appl Sci Manuf 2001;32:197–206. doi:10.1016/S1359-835X(00)00136-6.

Table 1. Test Matrix

Specimen Group	Nominal Pressure Rating (kPa)	No. of Specimens	Inner Diameter (mm)	Cross Sectional Area (mm^2)	Wall Thickness (mm)	Diameter-Thickness Ratio (DTR)	Filament Wind Layup (°)
P350-D76-C	350	5	76.2	416.5	1.7	44.8	$[\pm 55]_2$
P1050-D76-C	1050	5	76.2	964.4	3.8	20.1	$[(\pm 55)_2 / +55 / \overline{-55}]_S$
P350-D203-C	350	5	203.2	1741.5	2.7	75.3	$[\pm 55 / \overline{+55}]_S$
P700-D203-C	700	5	203.2	3103.0	4.7	43.2	$[\pm 55]_4$
P1050-D203-C	1050	5	203.2	4404.6	6.7	30.3	$[\pm 55]_5$
P350-D76-T	350	3	76.2	416.5	1.7	44.8	$[\pm 55]_2$
P1050-D76-T	1050	3	76.2	964.4	3.8	20.1	$[\pm 55]_7$

Note: Reported Wall Thickness is the entire wall thickness, including resin coat and liner, as reported by the manufacturer

Table 2. Test Results and Comparison with Analytical Results

Specimen Type	Pipe Modulus (GPa)				Strength (MPa)				Poisson's Ratio				Axial Strain at Peak Load, mm/mm ‡				Hoop Strain at Peak Load, mm/mm			
	Test AVE*	Test SD*	Model	Test/ Model Ratio	Test AVE	Test SD	Model	Test/ Model Ratio	Test AVE	Test SD	Model	Test/ Model Ratio	Test AVE	Test SD	Model	Test/ Model Ratio	Test AVE	Test SD	Model	Test/ Model Ratio
P350-D76-C	10.77	2.53	6.82	1.58	121.41	9.32	90.92	1.34	0.47	0.27	0.37	1.27	-0.0216	0.0034	-0.0269	0.80	0.0116	0.0014	0.0150	0.77
P1050-D76-C	9.04	0.57	8.32	1.09	128.86	8.71	96.74	1.33	0.46	0.07	0.38	1.21	-0.0249	0.0152	-0.0264	0.94	0.0109	0.0012	0.0150	0.73
P350-D203-C †	11.50	2.14	7.76	1.48	73.33	12.01	88.77	0.83	0.54	0.08	0.37	1.46	-0.0102	0.0023	-0.0287	0.36	0.0056	0.0016	0.0176	0.32
P700-D203-C	10.03	2.49	8.52	1.18	114.68	4.60	94.66	1.21	0.61	0.18	0.39	1.56	-0.0227	0.0029	-0.0263	0.86	0.0135	0.0015	0.0150	0.90
P1050-D203-C	8.32	0.91	8.82	0.94	117.20	4.09	95.86	1.22	0.46	0.10	0.39	1.18	-0.0307	0.0042	-0.0256	1.20	0.0169	0.0029	0.0145	1.16
P350-D76-T	8.68	0.20	6.60	1.32	47.48	1.76	51.6	0.92	0.43	0.04	0.36	1.19	0.0130	0.0061	0.0106	1.23	-0.0067	0.0016	-0.0040	1.66
P1050-D76-T	10.68	0.59	7.98	1.34	70.76	4.42	61.56	1.15	0.41	0.08	0.37	1.11	0.0136	0.0044	0.0111	1.23	-0.0052	0.0008	-0.0044	1.17
Average				1.27				1.20				1.28				1.04				1.07
SD				0.22				0.15				0.17				0.20				0.35

***** *AVE = Average; SD = Standard Deviation*
† *Premature failure due to local wall buckling*
‡ *Note that most axial strain gauges failed just before compression specimen ultimate failure and therefore the Axial Strain at Peak Load data presented here is approximate only.*

Table 3: Modeling Inputs in MPa

Property	Pure Epoxy	GFRP Lamina		
		Manufacturer Data	Modified Daniel & Ishai [20] (V_f = 50%)	Difference
E_1	2300	41369	37511	-9.3%
E_2	2300	8991	9496	5.6%
G_{12}	850	3228	3915	21.3%
ν_{12}	0.3	0.278	0.28	0.7%
ν_{21}	0.3		0.06	
S_{L+}	70		1036	
S_{L-}	94		564	
S_{T+}	70		35	
S_{T-}	94		116	
S_{LT}	43		81	

V_f =Fiber Volume Fraction; E_1 = Longitudinal Elastic Modulus; E_2 = Transverse Elastic Modulus; G_{12} = Shear Modulus; ν_{12} = Major Poisson's Ratio; ν_{21} = Minor Poisson's Ratio; S_{L+} = Longitudinal Tensile Strength; S_{L-} = Longitudinal Compressive Strength; S_{T+} = Transverse Tensile Strength; S_{T-} = Transverse Compressive Strength; S_{LT} = Shear Strength

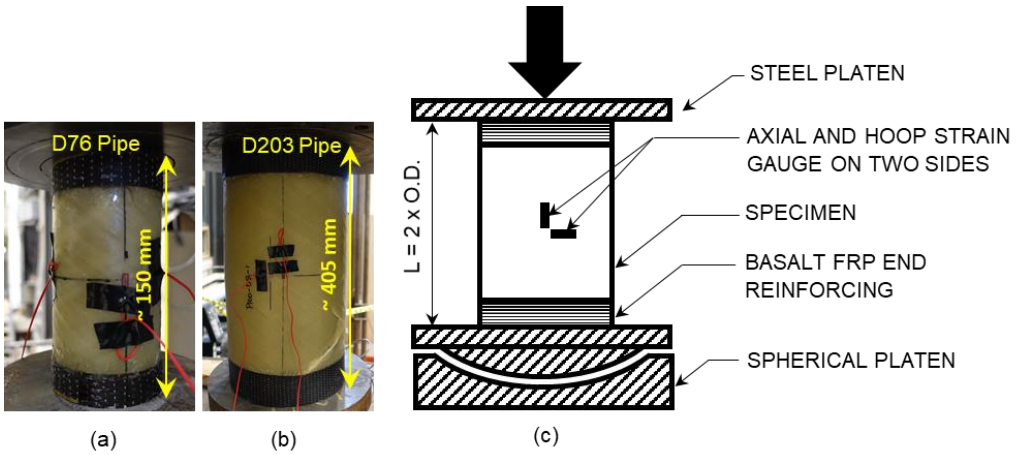

Figure 1: Compression Test (a) Sample D76 Pipe; (b) Sample D203 Pipe; and (c) Set-up

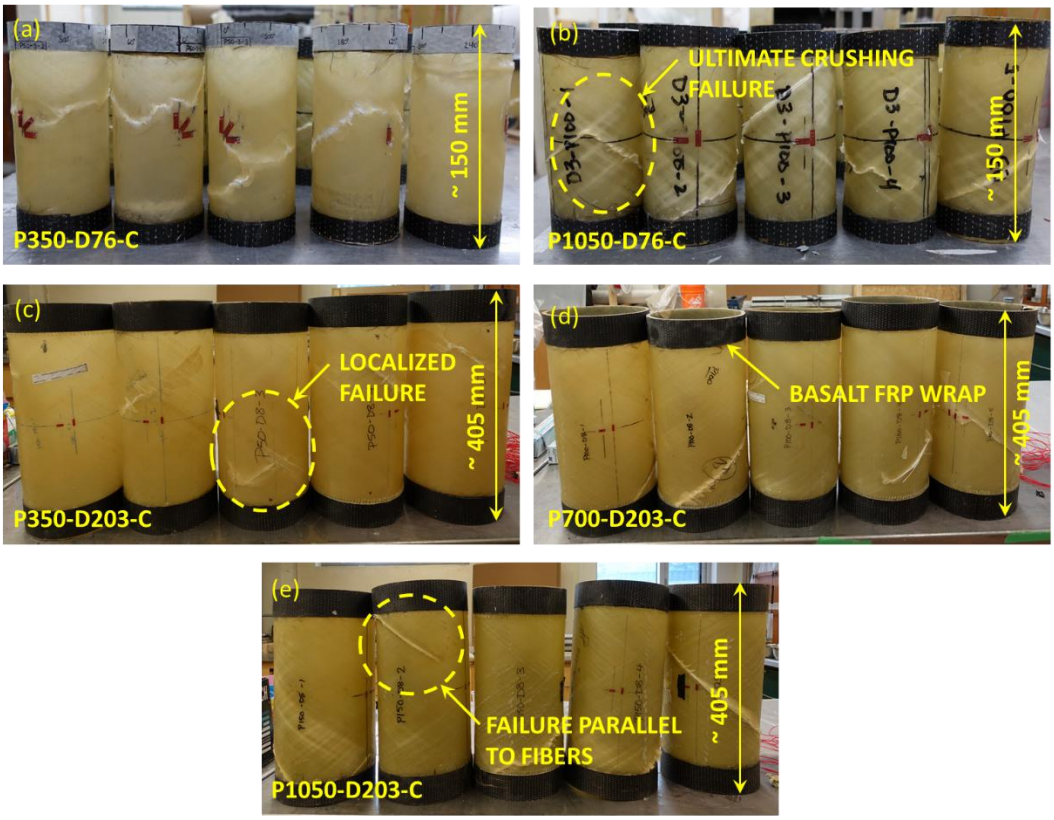

Figure 2: Compression Specimens: (a) P350-D76-C; (b) P1050-D76-C; (c) P350-D76-C; (d) P700-D203-C and; P1050-D203-C

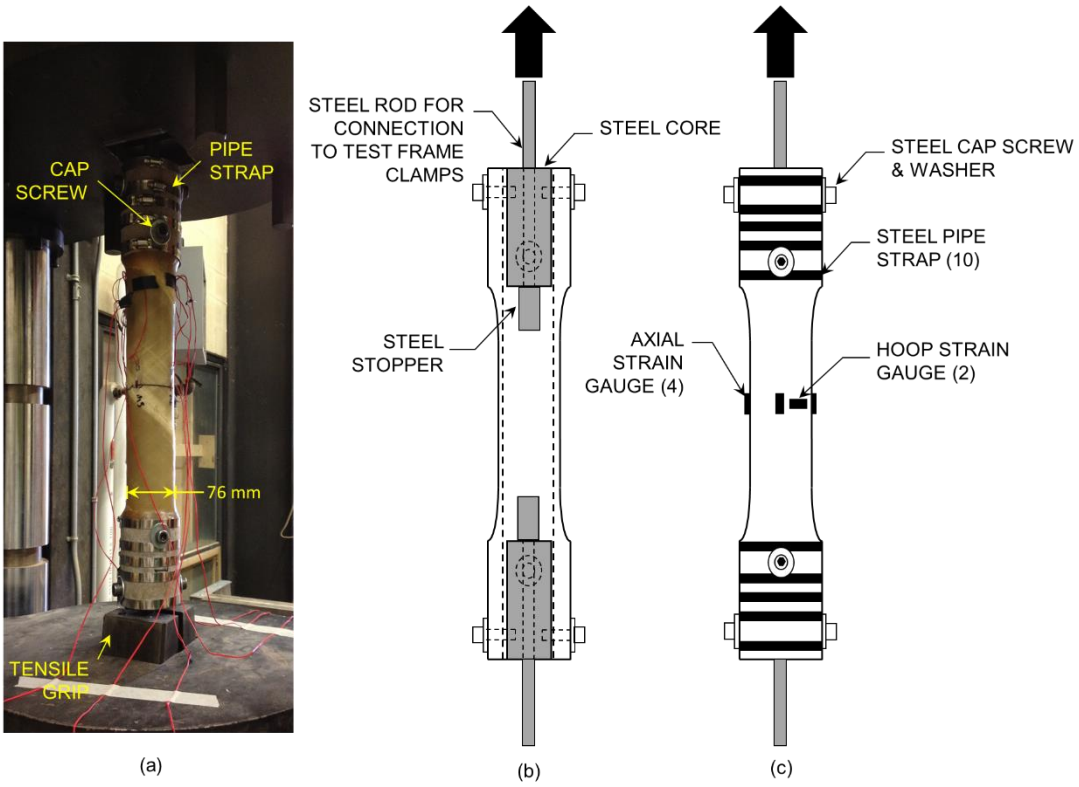

Figure 3: Tension Test (a) Photo of Tension Test; (b) Internal Schematic; and (c) External Schematic

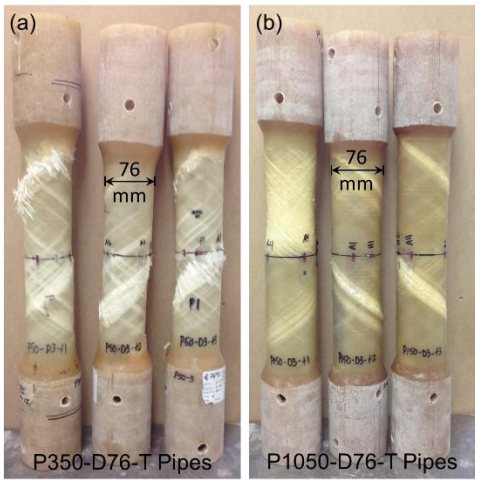

Figure 4: Tension Test Specimens (a) P350-D76-T and; (b) D1050-D76-T

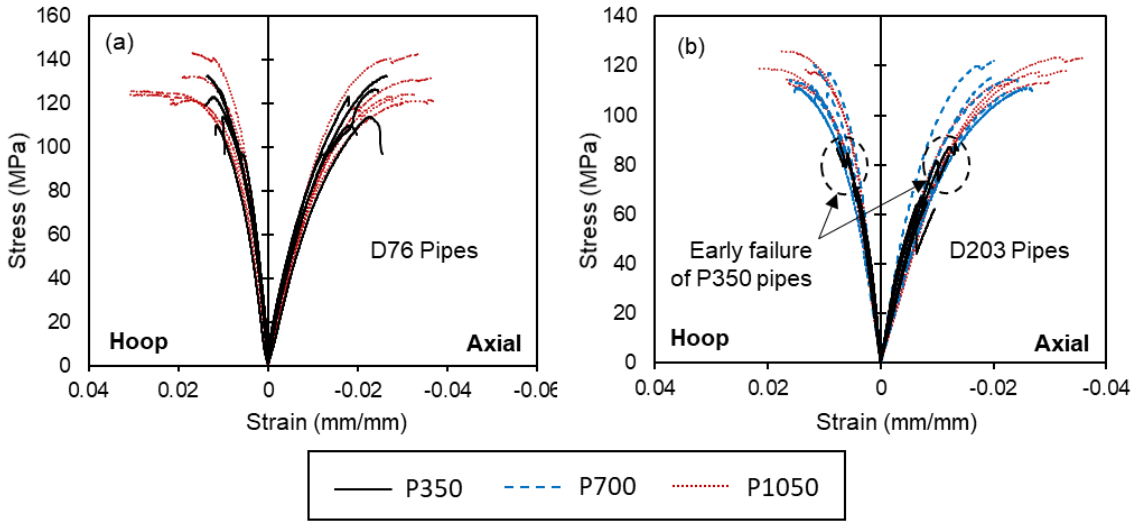

Figure 5: Stress-Strain Data – Compression Tests (a) D76 Pipes and; (b) D203 Pipes

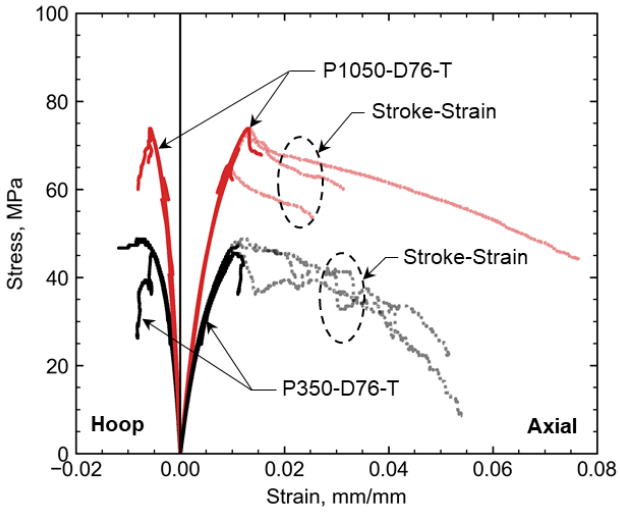

Figure 6: Stress Strain Data – Tension Tests

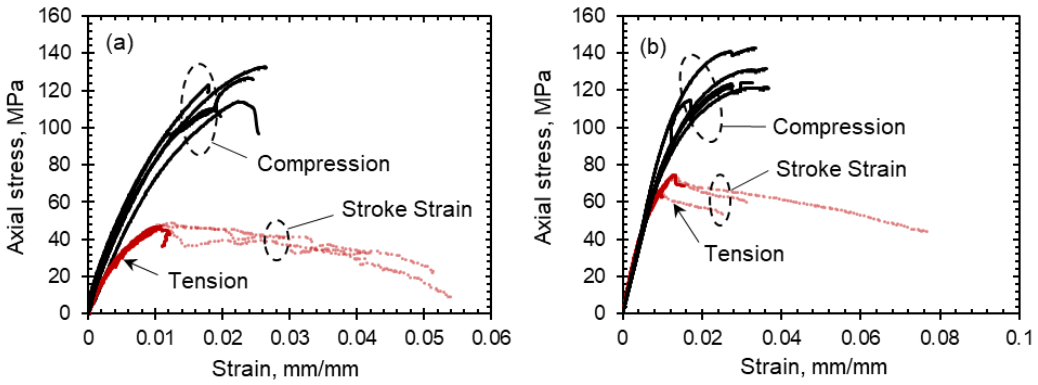

Figure 7: Comparison of Compression and Tension Axial Behavior (a) P350 Pipes and; (b) P1050 Pipes (Note that tension tests were terminated before ultimate failure)

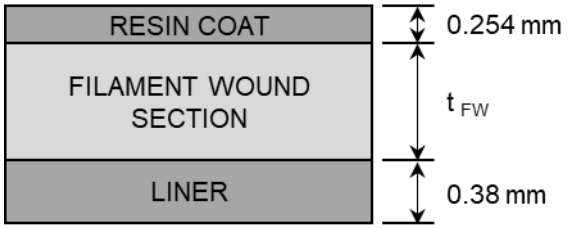

Figure 8: Pipe Architecture (Measurements Provided by Manufacturer)

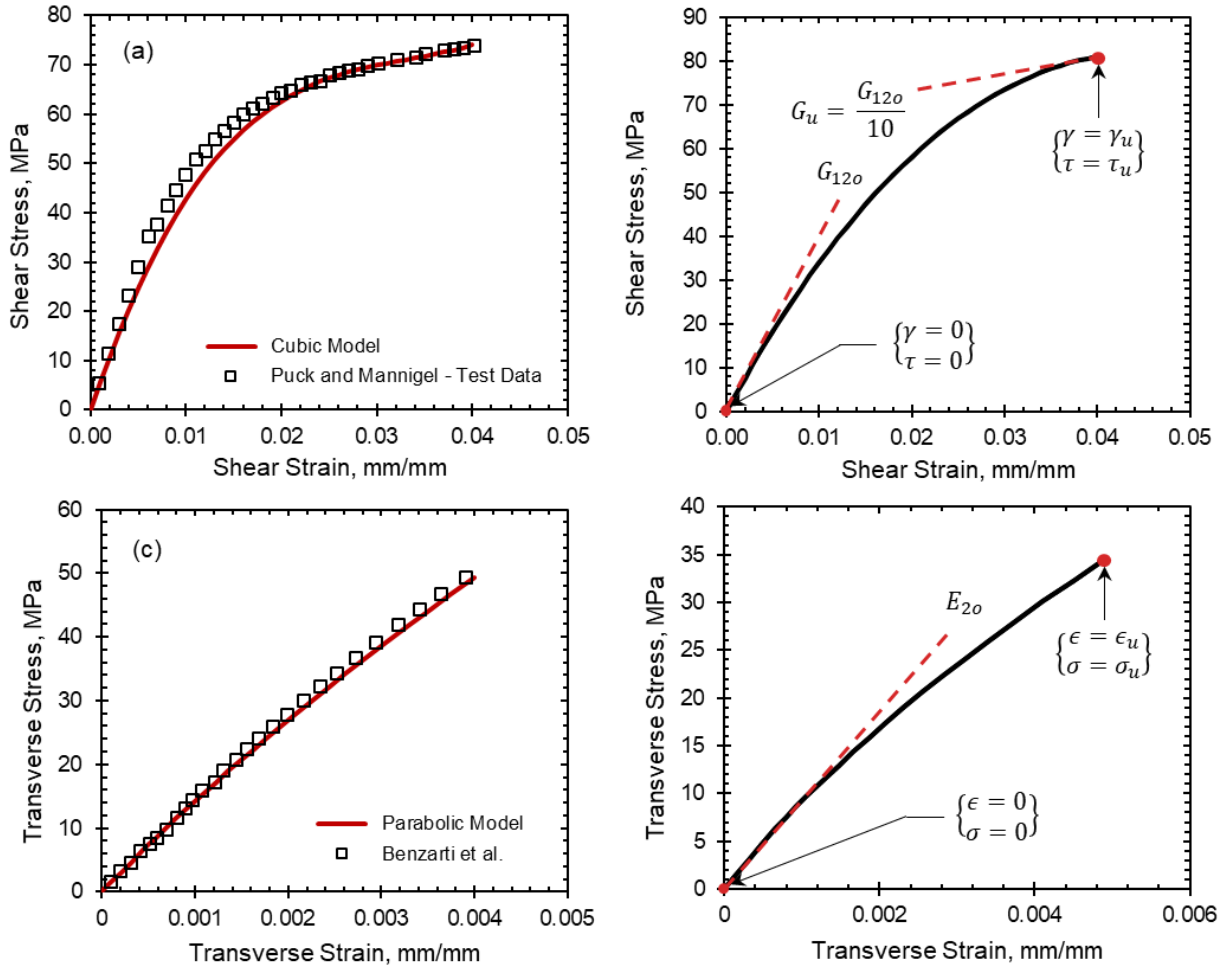

Figure 9: Constituent Stress-strain Behavior for Analysis (a) Verification of Cubic Model; (b) Cubic Model Used in This Study; (c) Verification of Parabolic Model and; (d) Parabolic Model Used in This Study

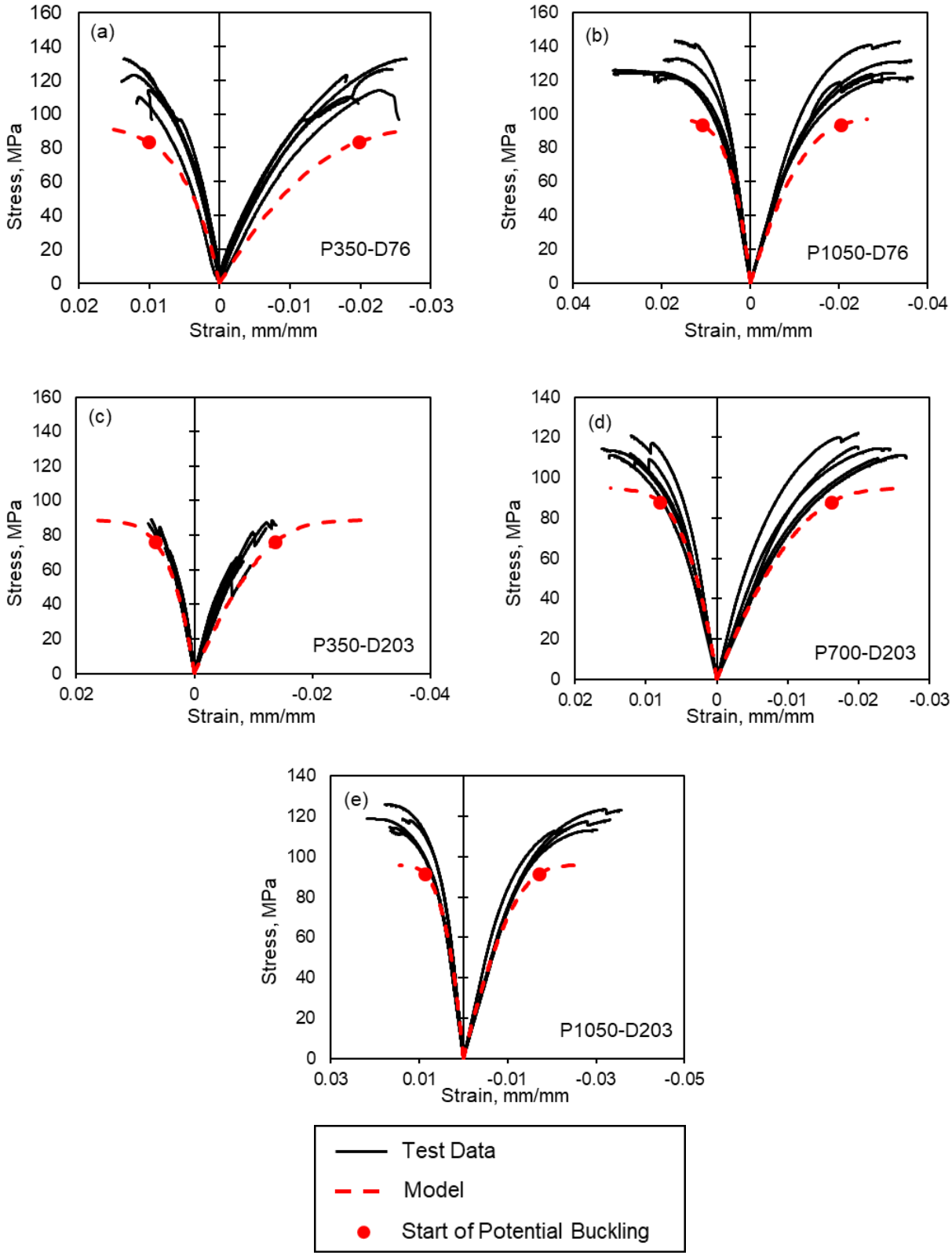

Figure 10: Compression Analysis (a) P350-D76-C; (b) P1050-D76-C; (c) P350-D76-C; (d) P700-D203-C and; P1050-D203-C

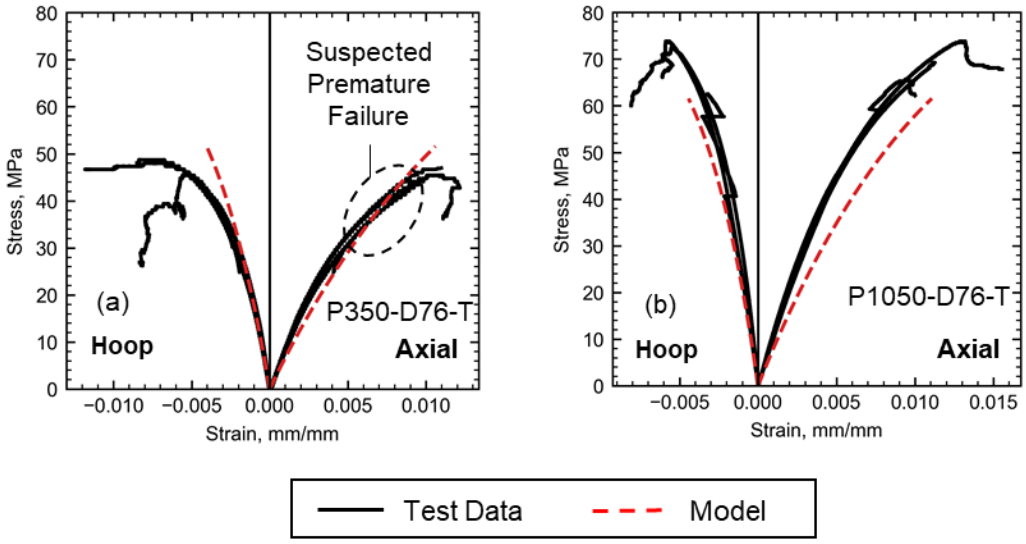

Figure 11: Tension Analysis (a) P350-D76-T and; (b) P1050-D76-T (Note: P350-D76-T Test Data is assumed to soften due to lack of fibers)

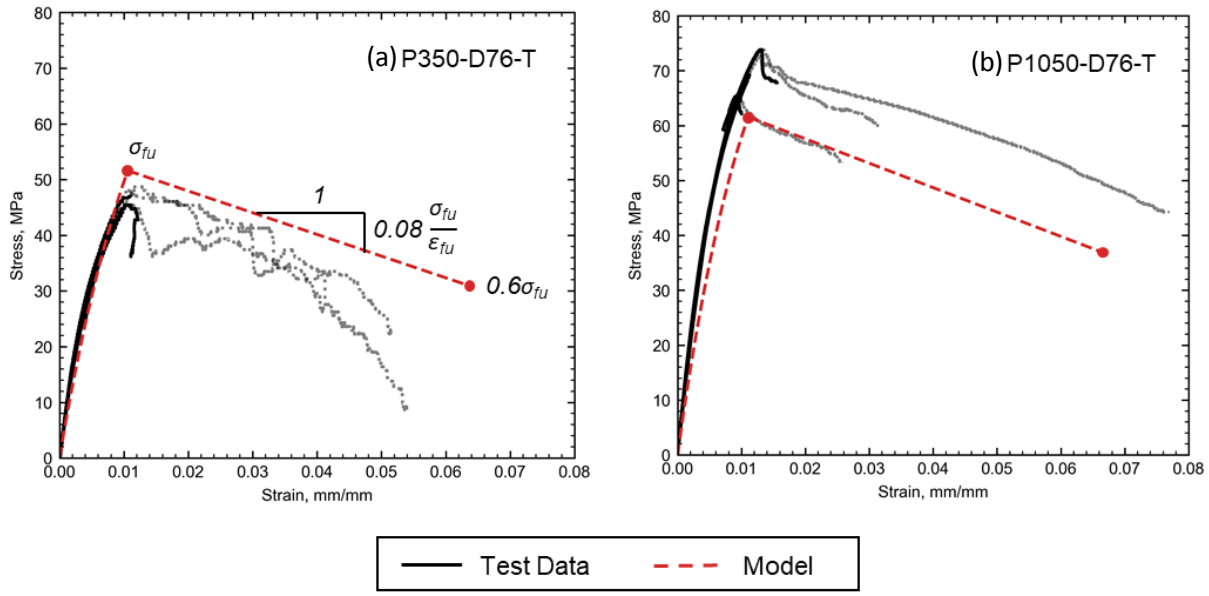

Figure 12: Post-Peak Modelling of GFRP Pipes in Tension (a) P350 and (b) P1050

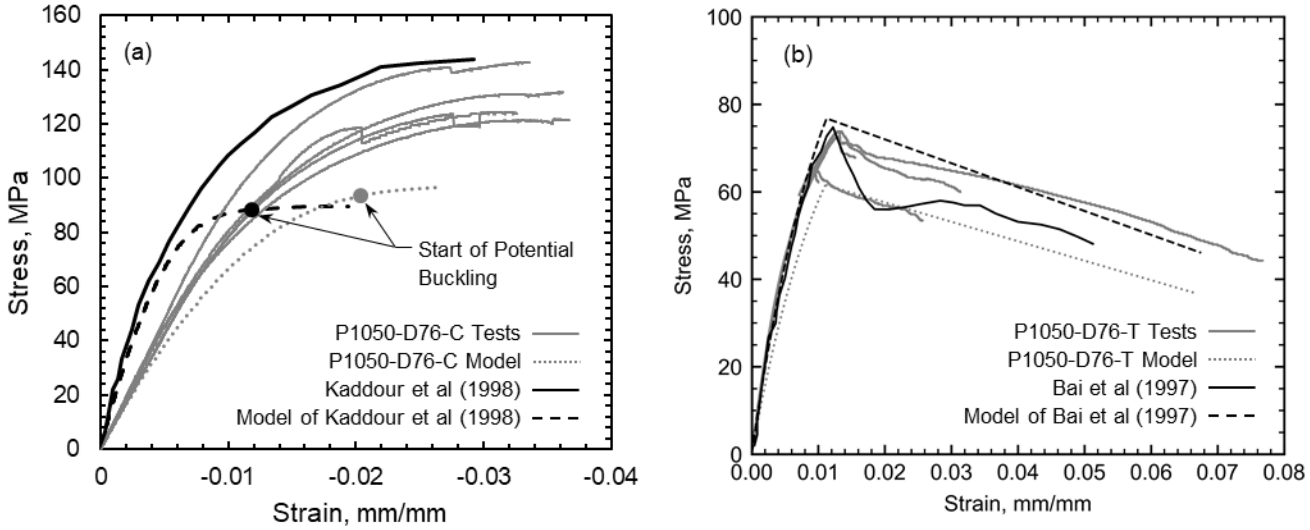

Figure 13: Model Verification with Data from the Literature (a) Compression Analysis and (b) Tension Analysis

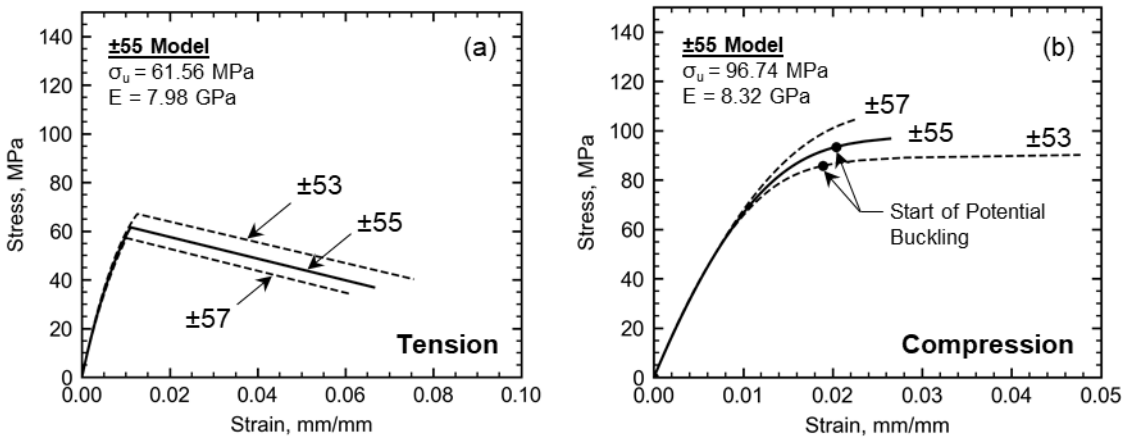

Figure 14: Effect of Manufacturer Fiber Angle Error on Stress-Strain Behavior of 76.2 mm Diameter Filament Wound GFRP Pipes (Based on Models for P1050-D76-T/C)